to absolute concentrations. Similarly, three-window images can be corrected for the effects of thickness by dividing by the low-loss image.

For EFIs, the best specimen and microscope parameters are usually similar to those for EELS. For example, as in EELS, the specimen should be very thin, i.e., $t/\lambda < 0.5$, and ideally about half this thickness.[17] A rule-of-thumb is that the plasmon peak should be no more than one-fifth the height of the zero-loss peak. Similarly, a small collection angle (5-10 mrad) is preferable because it usually increases the signal/background ratio of an edge (see Problem 4.9). Elements of atomic number greater than 12 allow a choice of edge energy for elemental analysis. It is best to use major edges, and those with threshhold energies from 100 to 1000 eV. At lower energies diffraction contrast and a steep background complicate quantification, and at higher energies the intensity becomes inconveniently low.

4.5.3 Chemical Analysis with High Spatial Resolution

Figures 4.19 and 4.20 illustrate several aspects of making chemical maps by EFTEM imaging. The experiment confirmed that Ag enrichment was responsible for the conventional contrast of two planes at the interface between an Ω-phase precipitate and an Al-rich matrix. The flatness of this internal interface was helpful for detecting chemical contrast at high spatial resolution.

The Ag $M_{4,5}$ edge has a delayed maximum, peaking about 50 eV above the edge onset (Fig. 4.19). For best intensity, the post-edge window should incorporate the intensity maximum of the absorption edge, but this required the pre-edge 2 image and the post-edge image to be recorded with a fairly large energy separation. This is not optimal for EFTEM imaging. Better detectability and spatial resolution can be achieved when the windows labeled "pre-edge 2" and "post-edge" abut together at the onset of an abrupt absorption edge. Abrupt K-edges or intense, sharp white lines at the L-edges of transition metals offer this possibility. Additionally, spatial resolution can be improved by using energy windows narrower than the 30 eV windows used in this example, provided sufficient signal is available. Nevertheless, the research problem involved Ag, so the windows for the energy filter were chosen as in Fig. 4.19.

Figure 4.20 shows a set of EFTEM images of an Ω precipitate plate in an Al-Cu-Mg-Ag alloy. To suppress diffraction contrast, the sample was tilted off the exact [011] zone-axis of the α-phase matrix, but the $\alpha|\Omega$ interfaces were still parallel to the electron beam. Two dark lattice-fringes can be seen at the $\alpha|\Omega$ interfaces on both sides of the Ω plate in the zero-loss image (Figs. 4.20a,b). These fringes are the width of two {111} Al planes (0.46 nm). At each interface, both the Ag jump-ratio image and three-window image show high-intensity lines. The three-window image is noisier than the jump-ratio

---

[17] Deconvolution of plural scattering is not possible in EFTEM because a full spectrum is not acquired.
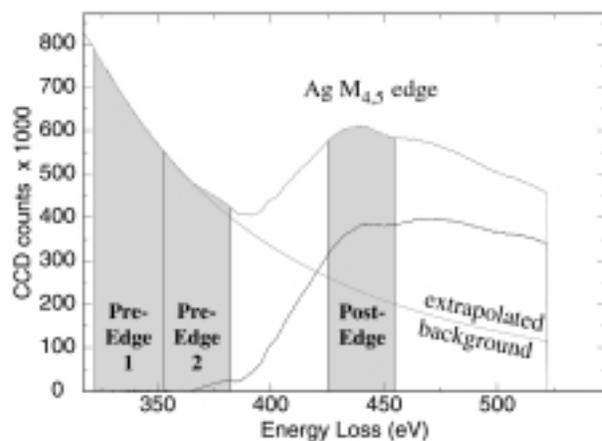
Fig. 4.19. A portion of an EELS spectrum showing the Ag $M_{4,5}$ edge and the placement of the pre-edge 1, pre-edge 2, and post-edge energy windows used for the EFIs in Fig. 4.20. An extrapolated background and a background-stripped Ag $M_{4,5}$ edge are also shown. After [4.8].

image, but provides a better estimate of the high enrichment of Ag. The background is featureless in both images, indicating that diffraction contrast and thickness effects are negligible. Two line profiles, acquired from the boxes shown in each image, are shown below the jump-ratio and three-window images. Both reveal segregation of Ag to the precipitate. These Ag layers are only 0.46 nm wide, showing the outstanding spatial resolution of the technique.

4.6 Energy Dispersive X-Ray Spectrometry (EDS)

4.6.1 Electron Trajectories through Materials

To understand how a high-energy electron causes the emission of characteristic x-rays from a specimen, we first need to understand some features of electron trajectories through specimens, and how to model the electron energy losses to inelastic processes. The simple model described here is useful for a physical understanding, but more complete models are available. In our simple model the electron trajectories through the solid are treated as straight lines between large-angle elastic scattering events. Along these straight paths we are interested in core electron excitations, since only these core ionization processes provide for subsequent x-ray emission.

We first consider the large-angle scatterings of electrons, which are primarily elastic in origin. The discussion of ionization cross-sections in Sect. 4.4.4 showed that the electron energy-loss spectrum tends to be forward-peaked, especially at small energy losses, owing to the ϕ-dependence of (4.43). Most inelastic processes in solids involve angles considerably smaller than the angles of elastic scattering, so we ignore the effect of inelastic scattering on the direction of the high-energy electron. Large-angle elastic scattering events
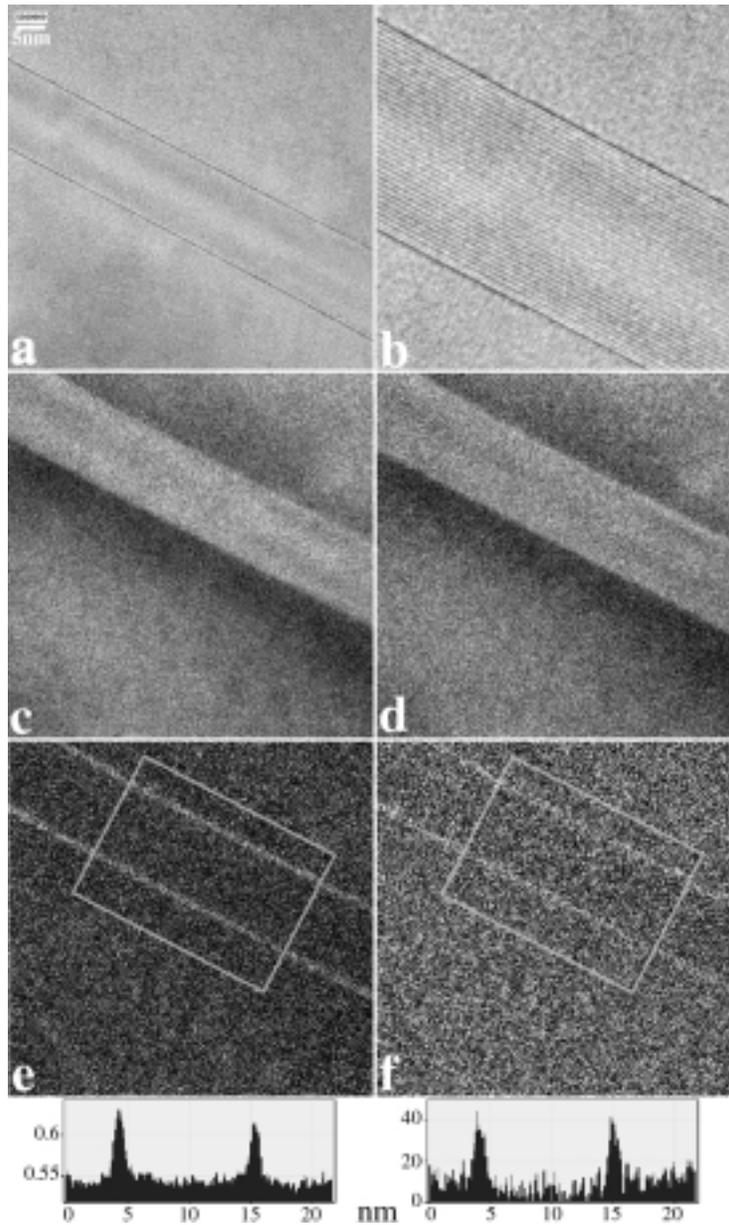
Fig. 4.20. A set of EFIs from an edge-on Ω-phase plate-shaped precipitate in an Al-Cu-Ag-Mg alloy (α-phase), acquired with the sample tilted so the habit-plane interfaces were parallel to the electron beam, but the sample was not directly on the zone axis. Some energy windows are shown in Fig. 4.19. (**a**) zero-loss image, (**b**) enlargement of part **a**, (**c**) pre-edge 2 image, (**d**) post-edge image, (**e**) Ag $M_{4,5}$ jump-ratio image, and (**f**) Ag $M_{4,5}$ three-window chemical map. Line profiles corresponding to **e** and **f** should be aligned along the short edge of the boxes enclosing the $\alpha|\Omega$ interfaces. ($\beta = 18$ mrad). After [4.8].